REPORT DOCUMENTATION PAGE

Form Approved
OMB No. 0704-0188

1. REPORT DATE *(DD-MM-YYYY)*	2. REPORT TYPE	3. DATES COVERED *(From - To)*
	Technical Paper	

4. TITLE AND SUBTITLE

5a. CONTRACT NUMBER

5b. GRANT NUMBER

5c. PROGRAM ELEMENT NUMBER
62500F

6. AUTHOR(S)

5d. PROJECT NUMBER
2308

5e. TASK NUMBER
M4S7

5f. WORK UNIT NUMBER
345382

7. PERFORMING ORGANIZATION NAME(S) AND ADDRESS(ES)

8. PERFORMING ORGANIZATION REPORT

9. SPONSORING / MONITORING AGENCY NAME(S) AND ADDRESS(ES)

Air Force Research Laboratory (AFMC)
AFRL/PRS
5 Pollux Drive.
Edwards AFB CA 93524-7048

10. SPONSOR/MONITOR'S ACRONYM(S)

11. SPONSOR/MONITOR'S NUMBER(S)

12. DISTRIBUTION / AVAILABILITY STATEMENT

Approved for public release; distribution unlimited.

13. SUPPLEMENTARY NOTES

See attached 13 papers, all with the information on this page.

14. ABSTRACT

15. SUBJECT TERMS

16. SECURITY CLASSIFICATION OF:			17. LIMITATION OF ABSTRACT	18. NUMBER OF PAGES	19a. NAME OF RESPONSIBLE PERSON
					Kenette Gfeller
a. REPORT	b. ABSTRACT	c. THIS PAGE	A		19b. TELEPHONE NUMBER *(include area code)*
Unclassified	Unclassified	Unclassified			(661) 275-5016

AIAA-96-2723

Investigation of Propellant Inefficiencies in a Pulsed Plasma Thruster

Gregory G. Spanjers, Keith A. McFall, Frank S. Gulczinski III, and Ronald A. Spores
Propulsion Directorate
OL-AC Phillips Laboratory
Edwards AFB, CA

32nd AIAA/ASME/SAE/ASEE Joint Propulsion Conference
July 1-3, 1996 / Lake Buena Vista, FL

INVESTIGATION OF PROPELLANT INEFFICIENCIES IN A PULSED PLASMA THRUSTER

Gregory G. Spanjers,[a] Keith A. McFall[b]
Frank S. Gulczinski III,[b] Ronald A. Spores[c]

Propulsion Directorate
OL-AC Phillips Laboratory
Edwards AFB, CA 93524

ABSTRACT

A Pulsed Plasma Thruster (PPT) [R.J. Vondra, J. Spacecraft **9**, 613 (1974)] benefits from the inherent engineering simplicity and reduced tankage fraction gained by storing the propellant as a solid. The solid is converted to the gaseous state during an electric surface discharge. Previous research [A. Solbes, J. Spacecraft **10**, 406 (1973)] has concluded that the bulk of the propellant expands gasdynamically from the chamber at low directed velocity, with possibly as little as 10% ionized and efficiently accelerated to high velocity using electromagnetic forces. The two velocity components result in a low propellant utilization efficiency. Critical to improving the PPT efficiency is preventing the formation of the low-velocity propellant and/or developing a means of accelerating it electromagnetically. In the present work measurements are made of the solid propellant conversion to the gaseous state with the intent of better understanding the formation process. By better understanding the propellant conversion it is hoped that future PPTs can be designed with significantly increased propellant efficiencies. The low-velocity component is observed through interferometric and broadband emission measurements. A high density neutral gas continues to vaporize from the propellant surface for at least 300 μs following the 25 μs current discharge. The neutral density is estimated to be 5 times the peak electron density, which is of the required magnitude for the neutral gas to be the major source of propellant inefficiency. Also observed are macroparticles emitting from PPT electrodes and propellant face after the current discharge. The macroparticles are believed to be molten material (either Teflon propellant or carbon deposited from previous discharges) thermally expelled from the surface by localized vaporization. The plume densities are measured for a range of PPT capacitances and energies. The plasma electron density is observed to increase linearly with energy. Compared with previous measurements [A. Solbes, J. Spacecraft **10**, 406 (1973)] that concluded the same dependance for total propellant usage, this implies that propellant efficiency cannot be improved by operating the PPT at higher energies (although increased energy efficiency can result, leading to an increased thrust efficiency).

I. INTRODUCTION

The Pulsed Plasma Thruster (PPT) has reemerged as an attractive electric propulsion option for small power-limited satellites. The PPT design[1] uses a solid Teflon propellant that is passively fed between the discharge electrodes by a linear spring. An integrated capacitor is discharged across the Teflon propellant face in an arc initiated by a lower energy sparkplug discharge. The main advantage of the PPT is the engineering simplicity which leads to high reliability. This reliability has been demonstrated by the successful application of PPTs in space missions starting in the late 1960s.[1,2,3]

By comparison to the related magnetoplasmadynamic (MPD) thruster,[4] the PPT would be expected to exhibit superior performance due to its high instantaneous power level. The short duty cycle enabled by the energy storage capacitor results in the PPT drawing 10's of Watts while charging (for typically 1 sec), and delivering Megawatts of power to the propellant during the μsec timescale discharge. This potential has not been realized. Operating near the optimal specific impulse (I_{sp}) for on-orbit applications[5] (1000 s - 2000 s), PPTs have achieved efficiencies of only 5% to 10%.[1,2,3,6]

Efficiency analysis, based on previous PPT research,[6,7,8] shows that the cause of the poor performance is divided approximately equally between low energy efficiency and low propellant utilization efficiency. The low propellant efficiency results from the formation of a multi-component plasma. A high-velocity component is efficiently accelerated electromagnetically to directed velocities between 30 km/s and 50 km/s. A low-velocity component is accelerated gasdynamically to directed velocities of approximately 3 km/s. The I_{sp}, ($I_{sp} = T^2/2mE$ using measured thrust (T), propellant usage per discharge

---

a) Principal Scientist, Hughes STX
b) Research Engineer, Member AIAA
c) Group Leader, USAF Electric Propulsion Laboratory, Member AIAA

(m), and discharge energy (E)), reached the optimal range (1000 s for the LES 8/9 PPT),[6,7] however the majority of thrust derived from a minority of mass in the high-velocity component.

In the present work, experimental measurements are directed towards furthering the understanding of the low propellant efficiency. Single-point interferometry quantifies the plasma density. High speed framing photography records the broadband plasma emission. Rogowski coils and high voltage probes monitor the PPT electrical parameters. The measurements are conducted for PPTs with capacitance ranging from 2 μF to 20 μF operated at energies ranging from 2 J to 80 J. These measurements show a high-electron-density plasma forming during each 1/2-cycle of the oscillatory PPT discharge. A high-density neutral gas is observed well after the PPT current has dissipated. The density of both components increases with increased energy and decreased capacitance. High-speed photography shows emission during the discharge suggestive of an ablative arc. Well after the discharge current has ceased, emission is observed suggestive of continued propellant vaporization. In addition, low-velocity (300 m/s) macroparticles are emitted from the propellant face and the electrode surface.

The neutral gas and macroparticles are concluded to be a major cause of the low propellant efficiency. Assuming the plasma electron density and neutral gas densities are proportional to the mass in the high-velocity and low-velocity components respectively, the measured relative density of the two components ($n_e/n_n \sim 1/5$ is of the magnitude required to explain the PPT propellant inefficiency. Assuming the electron density to be proportional to the mass of the high-velocity component, the linear scaling of the maximum electron density, coupled with previous measurements showing the same scaling for the total mass usage,[8] implies that increasing the discharge energy will not increase the propellant efficiency. The increased efficiency and thrust documented at higher discharge energies[7] is attributable to an increased velocity for the fast component which raises the energy efficiency.

Measurements at a fixed energy show significant increases in electron density with decreased capacitance (and associated increased voltage). If the propellant usage in these cases is approximately equal, the measurements imply that increased propellant efficiency may be achieved by reducing the PPT capacitance.

II. EXPERIMENTAL APPARATUS AND DIAGNOSTICS

The experiments are performed in Chamber 5 of the Electric Propulsion Laboratory at Phillips Laboratory, Edwards AFB. Chamber 5 is a new facility, currently in fabrication, optimizing diagnostic accessibility during tests on low-power electric thrusters. The chamber is 1.2 m in diameter and 1.8 m in length. Presently the chamber is evacuated using a 1400 l/s turbomolecular pump backed by a rotary mechanical pump. Base pressures of 3×10^{-5} Torr are typical. Once completed, the system will be evacuated by two 1400 l/s turbomolecular pumps backed by a 2-stage mechanical pump (1420 l/m). The completed facility is expected to achieve base pressure in the 10^{-7} Torr range.

During tests the thruster is affixed to an acrylic plate for electric isolation from the chamber. The chamber is floated electrically to prevent the plasma current conduction to the chamber walls experienced in previous PPT research.[6]

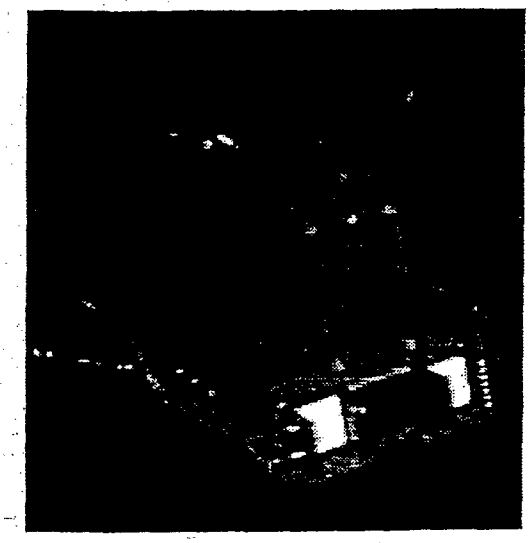

Fig. 1 XPPT-1 Pulsed Plasma Thruster

A. Pulsed Plasma Thruster

The experiments were performed on XPPT-1 (Experimental Pulsed Plasma Thruster #1), a PPT thruster designed and fabricated in-house. The XPPT-1, shown in Fig. 1, is similar to the LES 8/9 PPT[6,7] electrically and geometrically, but has increased diagnostic access. The stripline (approximately 50 nH), electrode dimensions (2.5 cm x 2.5 cm), electrode separation (2.5 cm), and fuel bar geometry (2.5 cm x 2.5 cm) are identical to that used in the LES 8/9 design. Sparkplugs used to initiate the discharge are identical to those from LES 8/9 (actually leftovers from the original program). Several major differences exist between the XPPT-1 and LES 8/9 designs. In the LES 8/9 PPT the two electrode sets were directed at opposing 30° angles to facilitate thrusting in different directions. This was done to increase the PPTs usefulness in the LES 8/9 stationkeeping application. The 30° thrust angle has been removed in the XPPT-1 design. The housing around the electrodes in the LES 8/9 design has been eliminated to provide diagnostic access. The electrodes in XPPT-1 are both fabricated from 304 Stainless Steel, while Mallory 1000 (thoriated tungsten) and 17-4 Steel were used for the LES 8/9 cathode and

anode respectively. Modifications to the interface between the capacitor and the stripline in the XPPT-1 design has resulted in the ability to easily attach and test a wide range of capacitors of various size and geometry. In addition, these modifications allow for a low inductance Rogowski coil connection to directly monitor the PPT current (Ion Physics CM-1-L).

The XPPT-1 capacitor is charged using a laboratory power supply. High voltage (both charging and transient during the discharge) are measured using a Tektronix 6015 1000X high-voltage probe connected at a break in the coaxial charging line external to the vacuum chamber. The sparkplug is discharged using a similar current pulse characteristics as that used in LES 8/9. A 2 μF capacitor charged to 600 V is discharged through a 1:3 voltage step-up transformer to the center pin of the sparkplug. The sparkplug is grounded directly to the PPT cathode. The discharge initiation circuit is adapted from a milli-pound PPT (prior to modifications this was identical to the circuit used in LES 8/9).[9] Discharge is alternated between the two sparkplugs via a manually operated relay external to the vacuum chamber. Only one of the two fuel bars is discharged during the present measurements.

Twelve channels of data are recorded on a set of three Tektronix 460A Digitizing Oscilloscopes (100 Mhz sample rate, 350 MHz bandwidth).

B. Diagnostics

The interferometer uses a heterodyne quadrature technique.[10] An acousto-optic modulator (Bragg cell) splits the 35-mW HeNe laser (633 nm) into reference and scene beams with a 40 MHz shift in the reference beam to facilitate heterodyne phase detection.[11] The scene beam is passed through the plasma parallel to the electrodes and fuel bar face at specified measurement locations. The beams are recombined, attenuated (~3 ND) and directed to the active area of a photodiode. Attenuation is variable and adjusted to keep the photodiode/amplifier below saturation. The photodiode current is amplified at 100 kV/A, filtered at 40 MHz with a 10 MHz bandpass and analyzed using an analog phase detection system with 10.7 MHz filtering, as shown in Fig. 2. The detection system was assembled in-house from discreet analog components (detector, amplifier, power splitter, double-balanced mixers, and filters).

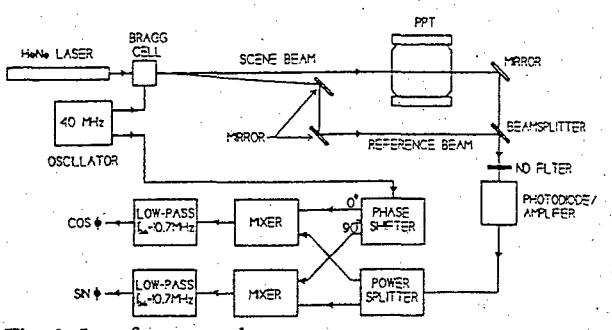

Fig. 2 Interferometer layout.

Phase shift of the scene beam results primarily from plasma electrons and, to a lesser degree, neutral gas. The phase shift can be expressed as

$$\Delta\phi = \frac{2\pi}{\lambda}\int(1-N_e)dl + \frac{2\pi}{\lambda}\int(1-N_n)dl \qquad (1)$$

where N_e is the refractive index due to the plasma electrons and N_n is the refractive index due to neutrals. The electron index is $N_e = (1-\omega_p^2/\omega^2)^{1/2}$ where collisional damping has been neglected by assuming that the collision frequency is much smaller than the laser frequency. The refractive index for the neutrals is more difficult to calculate. The composition of the neutral gas expelled from the PPT is unknown although, based on gas analysis of chamber residuals after a PPT discharge,[12] it is expected to be a combination of carbon, fluorine, and various radicals. Further complicating the calculation is that the refractive indices for these materials are well tabulated for the solid but generally unknown for the vapor. A rough estimate of the neutral refractive index is calculated using the Gladstone-Dale equation.[13]

$$N_n = 1 + \rho\sum_i a_i K_i \qquad (2)$$

where ρ is the mass density, a_i is the mass weighted fractional concentration of component i, and K_i is a specie constant. By comparison to low-atomic-number gaseous elements, $(K_{CO_2} = 0.23x10^{-3}\,m^3/kg$, $K_{N_2} = 0.24x10^{-3}\,m^3/kg$, $K_{O_2} = 0.19x10^{-3}\,m^3/kg)$[11] the mass weighted summation over the specie constants for the mixture of neutrals expected in the PPT plasma is estimated to be 0.22 x 10^{-3} m^3/kg. The approximation of the neutral index of refraction is completed by using a weighted average $(m = (2m_C + 4m_F)/6$ to calculate an effective mass density in Eq. (2). The expected interferometric phase shift for a mixture of plasma and neutrals is then (MKS units in degrees)

$$\Delta\phi = 2.8x10^{-15}\lambda\int n_e dl - \frac{3.9x10^{-29}}{\lambda}\int n_n dl \qquad (3)$$

For λ_{HeNe} = 632.8 nm the phase shift resulting from the electrons is 29 times that arising from an equal density of neutral gas.

To simultaneously resolve the densities of the electrons and neutral requires two laser frequencies. In the present experiment, using a single laser frequency, a large negative phase shift is observed in the early stages of the discharge, indicative of a high electron density. Analysis at this time assumes the absence of significant phase shift from the neutral density. The accuracy of the electron density measurement at this time is supported by the much higher index for the electrons. Long after the discharge

Spatial resolution of the measurement is set by the 0.5 mm active area on the photodetector. The laser beam is not focussed, which increases the spatial resolution at the expense of signal intensity. Refractive effects act to bend the light path, changing the location of the measurement from that chosen during laser alignment. Assuming a parabolic density profile, the maximum refractive angle is $\alpha_{max} = \sin^{-1} n_{max}/n_c$ where $n_c = \varepsilon_o \omega^2 m/e^2$ is the plasma cutoff density. The maximum electron density observed in the present experiments is 3.0×10^{16} cm^{-3}. With the photodetector 2.5 m from the plasma, this corresponds to a maximum deflection of 30 μm, an order of magnitude less than the spatial resolution of the system.

Light emission from the plasma is recorded digitally using a high-speed, framing camera (Stanford Computer Optics 4 QUIK 05). The camera has a minimum 50 ns gate time and an image intensifier for measuring low light signals. Sensitivity increases exponentially with intensifier gain.

III. THEORY

The importance of understanding and eventually improving the propellant utilization efficiency in a PPT becomes clear with simplified estimations of the performance in LES 8/9. The LES 8/9 performance parameters[6,7] for a single discharge are tabulated in Table 1.

Table 1: LES 8/9 Performance Parameters[5,6] for a Single Discharge

Thruster Energy	E_o	25 J
Specific Impulse	I_{sp}	1000 s
Thrust	T	300 μN
Propellant Mass	m	28.5 μg
Thrust Efficiency	η	6.3 %
PPU Efficiency	η_{PPU}	80 %

Previous experiments have shown the presence of several plasma components with varying velocities.[14] Generally these can be grouped into two groups: a high-velocity plasma with a $v_{fast} \cong 40 km/s$, and a low-velocity gas with a $v_{slow} \cong 3 km/s$. Simplifying the analysis to these two groups allows the performance parameters to be separated by group, as tabulated in Table 2.

Table 2: LES 8/9 Performance Separated for Two Velocity Groups

		Fast	Slow
Mass (μg)	m_i	6.0	22.5
Thrust (μN)	T_i	234	66
Kinetic Energy (J)	KE_i	4.6	0.1
Formation Energy (J)	$m_i \Phi_i$	0.7	2.6

In Table 2, the Formation Energy ($\Phi = 0.116 J/\mu g$) assumes for both groups that the Teflon is fully vaporized and disassociated and that each of the resultant 2 carbon and 4 fluorine atoms are singly ionized. This underestimates the formation energy for the fast group since highly ionized atoms have been observed,[15] and overestimates the formation energy for the slow group since neutrals are observed in the present work. Although this estimate probably results in the total formation energy being overestimated (since 79% of the mass is in the slow group), 60% of the initial energy remains unaccounted for.

From the values in Table 2, the energy (or acceleration) efficiency is calculated as:

$$\eta_E = \frac{KE_f + KE_s}{\eta_{PPU} E_o} = 23.5\% \tag{4}$$

The propellant utilization efficiency is calculated as:

$$\eta_p = \frac{T^2}{T_f^2 + T_s^2 + m_f m_s (v_f^2 + v_s^2)} = 32.5\% \tag{5}$$

The total efficiency is the product of the three efficiencies:

$$\eta = \eta_{PPU} \eta_E \eta_p = 6.1\% \tag{6}$$

From this analysis it is clear that the inefficiency associated with the mass usage is comparable to that associated with the energy.

The energy and propellant efficiencies are linked. For example. If the low-velocity gas was prevented from forming, presumably the 2.6 J of formation energy would also be recovered and both efficiencies would increase. Thus research directed at understanding the plasma and neutral gas formation processes are critical to achieving significant improvement in PPT performance.

A. Propellant Ablation Model

During propellant transformation from solid to gas, the PPT is similar to an ablation controlled arc (ACA). Radiation from the arc induces wall ablation (boiling) from the propellant face. The outstreaming of vaporized propellant provides convective cooling. A neutral gas vapor shield forms between the plasma arc and the solid propellant, attenuating the transport of the arc radiation to about 1/3 for Teflon.[16] In this model the ablated mass from the PPT is proportional to the electric energy dissipated ohmically in the arc.

$$m \propto R \int_0^\infty I^2 dt \tag{7}$$

where R is the effective plasma resistance.

For the cylindrical geometry of ACAs, the constant of proportionality can be determined from the transmissivity of the vapor shield and the material properties of Teflon. In the PPT, calculation of arc radiation incident on the propellant surface is complicated by the planar geometry and the uncertainty in the arc position relative to the wall.

A similar model was applied to the PPT by Solbes and Vondra[8] (independent of and preceding the ACA research). Their model incorporated essentially the same physics as the ACA model and includes effects resulting from the changing inductance during plasma acceleration. Excellent agreement was found between theory and measured ablation rates for capacitances ranging from 0.67 μF to 6 μF and voltages from 500 V to 2000 V (12 J maximum).

For the present work, the mass fraction in the fast component is investigated by measuring the plasma electron density during the discharge, and assuming proportionality between the two. For a given circuit, the total mass ablated will scale linearly with energy according to the ACA[15] model, and the model and experimental data of Solbes-Vondra.[8] By characterizing the scaling of the electron density with energy, the operating energy with the highest propellant efficiency can be determined for a given circuit.

IV. EXPERIMENTAL MEASUREMENTS

Experiments were performed for the PPT capacitor and energy configurations listed in Table 3. Measurements at higher energy were precluded by high-voltage breakdowns. Approximately 20 density measurements were performed at each setting. Half of these were recorded with a 10 ns digitizing speed. to maximize temporal resolution during the discharge. and half recorded with a 40 ns digitizing speed, to increase the total time base enabling measurements of neutral gas well after the discharge. In both cases the record length was 5000 data points for total time bases of 50 μS and 200 μs.

Measurements of the mass ablated per discharge at each experimental parameter are presently being performed and are not presented here.

Figure 5 shows the voltage and current characteristics of the PPT for a 20 J discharge and the three different capacitances. The PPT current, Fig. 5a, shows the currents in the 3 cases to be approximately equal indicating a relatively uniform total circuit inductance. The decay time of the energy is relatively equal indicative of constant L/R between the three cases. This implies more oscillations, or equivalently a higher voltage reversal, for the 2 μF case as observed in Figs. 5a and 5b. Figure 5b, PPT voltage, shows the higher voltages required for smaller capacitances at constant energy. Comparison of Figs. 5a and 5b show that a calculated $I = C\frac{dV}{dt}$ does not agree well with the current measured with the Rogowski probe, especially during the first 2 μs of the discharge. This probably results from two perturbations in the voltage measurement. First, by measuring the voltage at a break in the charge cable, there is effectively an inductor between the capacitor and the voltage probe. The probe will measure voltages due to changing currents across this inductor. Second, the high voltage supply remains connected during the discharge. DC offsets observed in the voltage measurement may be due to the charging of capacitors within the power supply.

Table 3: PPT Experimental Parameters

Capacitance	Voltage	Energy
2 μF	1450 V	2.1 J
	3000 V	9 J
	4470 V	20 J
10 μF	632 V	2 J
	1414 V	10 J
	2000 V	20 J
	2830 V	40 J
	3461 V	60 J
	4000 V	80 J
20 μF	633 V	4 J
	1000 V	10 J
	1414 V	20 J
	2000 V	40 J
	2449 V	60 J
	2828 V	80 J

Figure 5c shows the density measured in the three cases. For a fixed energy higher electron densities are observed for the smaller capacitance. At later times the density for the 2 μF case is negative. This indicates a positive phase shift resulting from high neutral gas densities. The positive phase shift is more apparent at times well after the discharge has terminated. Figure 6 shows the density on a time base extending 180 μs from the initiation of the 25 μs discharge. The neutral density is observed earlier in the discharge, and has a faster rise for the PPT with smaller capacitance.

The presence of a high-density neutral gas 150 μs after the discharge is supported by broadband optical emission measurements. Figure 7 shows intensified photographs at several times during the discharge. The photos show the PPT electrodes side-on with the cathode on the bottom. Relative scale can be inferred from the 2.5 cm electrode separation. Figure 7a is recorded at time t=0 with a 10 μs shutter. Emission suggestive of the stationary ablative arc is observed. Assuming that high emission corresponds to areas of high current density, the current flows in an arc separated from the propellant face by a slightly darker region. The darker region is presumably the vapor shield of neutral gas expanding from the Teflon face. Images with shorter exposure time during the initial discharge show structure similar to Fig. 7a. At no time is an arc observed displaced down the electrodes, as would be expected with a slug of plasma accelerated electromag-

netically. The main plasma arc remains near the Teflon face while less emissive, presumably more tenuous, plasma often extends out the electrodes, as seen in Fig. 7a. The arc intensity oscillates with current oscillations, becoming dark at each current zero-crossing and bright at each current maximum. Emission at times well after the current flow is suggestive of boiling from the Teflon surface. Figures 7b, 7c and 7d are the emission recorded at 100 μs, 200 μs and 300 μs with shutter times of 10 μs. The source of the emission is believed to be excited neutral atoms (near the Teflon face) and molten macroparticles (in isolated emissive spots away from the propellant). To discern particle motion, Fig. 8 was recorded at 200 μs with a longer gate time (100 μs). The light emitting material appears as streaks. Comparing the length of the streaks with the gate time implies velocities of approximately 300 m/s.

In Fig. 9 the maximum electron density during the discharge and the neutral density at 180 μs are plotted as a function of the initial capacitor energy. Based on Eq. (7), the data should be plotted as a function of $\int i^2 dt$ for comparison to ACA theory. Calculations show $\int i^2 dt$ to be proportional to discharge energy for the present data set. Since the functional dependencies are the same, the density data is plotted as a function of discharge energy to increase its usefulness in PPT design. For each case, with varied PPT capacitance, both the neutral and plasma density increase linearly with charge energy. Both densities also increase with decreased capacitance. Note that it is not clear whether the neutral density is highest for the 2 μF case or if it simply has a faster rate of increase. It is apparent from Fig. 6 that the neutral density rises faster for the low capacitance case and slower for the high capacitance case. Lacking the diagnostic capability to monitor the density returning to 0, it is not possible to determine which configuration results in the highest neutral density.

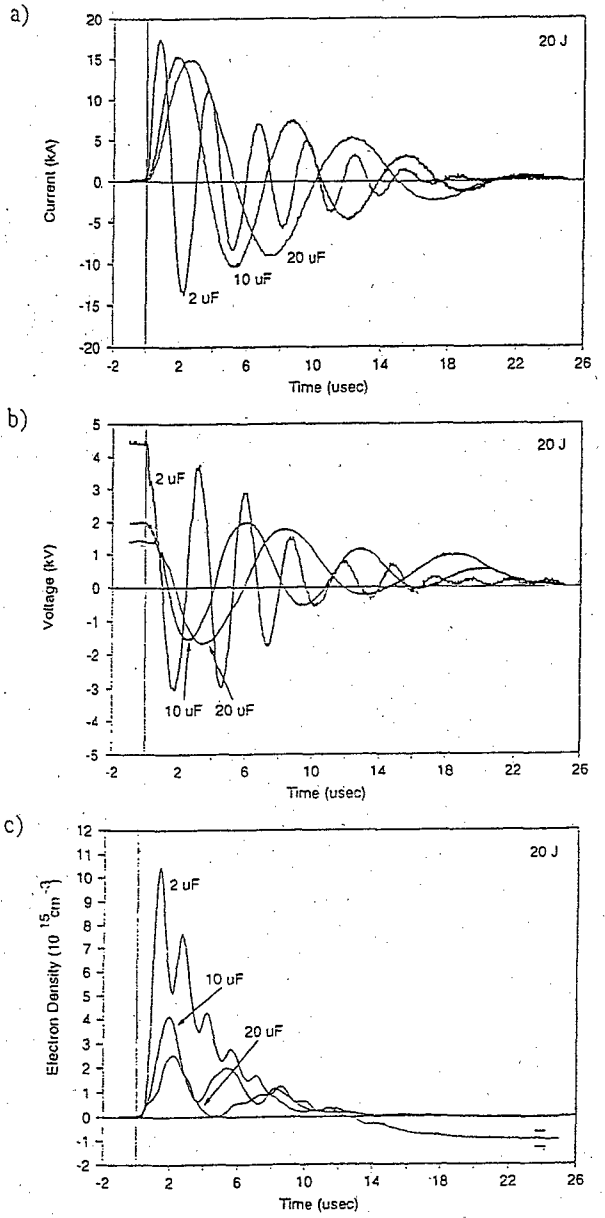

Fig. 5 Characteristics of the PPT discharge: a) Current, b) Voltage, c) Electron density.

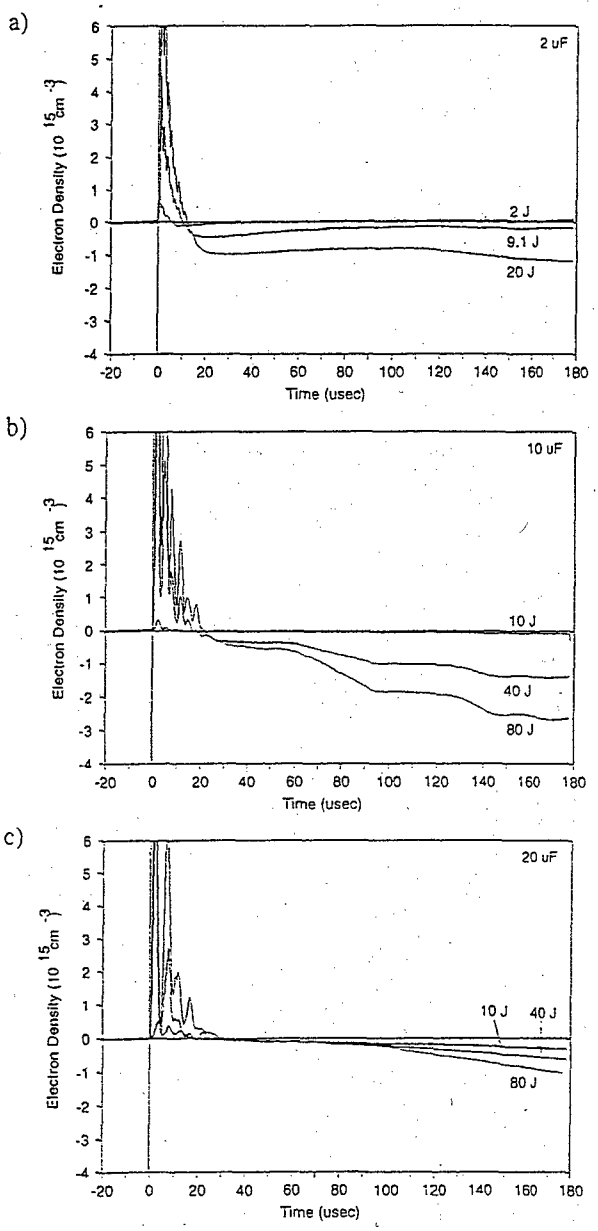

Fig. 6 PPT density on long time base. a) is the density for the 2 μF case, b) the 10 μF case, and c) the 20 μF.

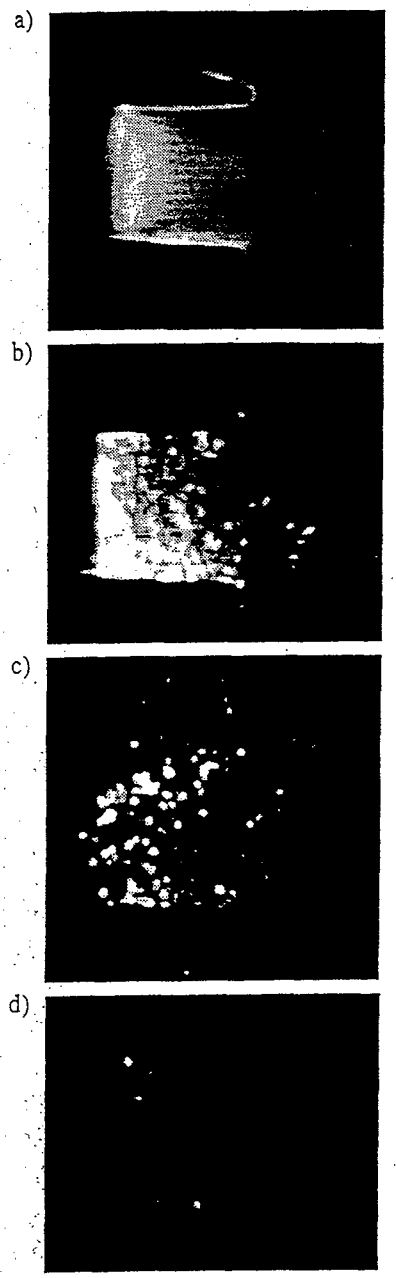

Fig. 7 Intensified light emission from the 20 μF, 20 J PPT with a 10 μs exposure time. a) Emission at t=0 μs with gain 300; b) Emission at 100 μs with gain 800; c) Emission at 200 μs with gain 800; and d) Emission at 300 μs with gain 750.

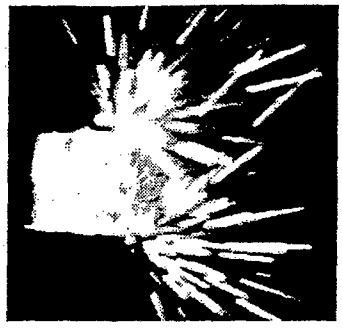

Fig. 8 Emission at 200 μs with a 100 μs exposure time (gain=700) showing streaks indicative of particles with velocities of approximately 300 m/s.

V. DISCUSSION

The neutral gas and macroparticles are indicators of the low propellant efficiency since efficient electrodynamic acceleration of these components is impossible. From Fig. 9, the neutral density is roughly 5 times the maximum electron density, independent of the circuit parameters. Note that previous line emission measurements[14] have shown the presence of some triply-ionized atoms. Thus the measured electron density may be several times greater than the associated ion density. The mass ratio between the two groups is the density ratio multiplied by the average plasma ionization. The mass ratio implied by comparing the densities of the electrons and the neutrals could therefore range from 5 to 15. Previous researchers have estimated the mass in the low-velocity component to be 9 times the mass in the high-velocity component.[14] The calculations used to construct Table 2 estimate the low-velocity mass to be 4 times the high-velocity mass. Thus the densities of the neutral gas and plasma electrons are in relative agreement with estimates for the magnitudes of the masses in the 2 velocity components.

The macroparticles are believed to be ejected from the propellant and electrode surfaces as a result of localized high temperature areas. In the case of ejection from the electrodes, particle ejection can result from propellant residue from previous discharges (presumably carbon). Since carbon has a sublimation temperature in excess of the vaporization temperature of steel, the steel electrode material can vaporize underneath the carbon, and create a high pressure gas which ejects the carbon coating as a macroparticle. In the case of ejection observed from the propellant face, the previous theory is also applicable for carbon deposits on the propellant face. In addition it is possible for radiation from the arc to deposit its energy well below the propellant surface.[15] In this case localized vaporization occurs behind the Teflon face causing similar ejection of face material as a macroparticle.

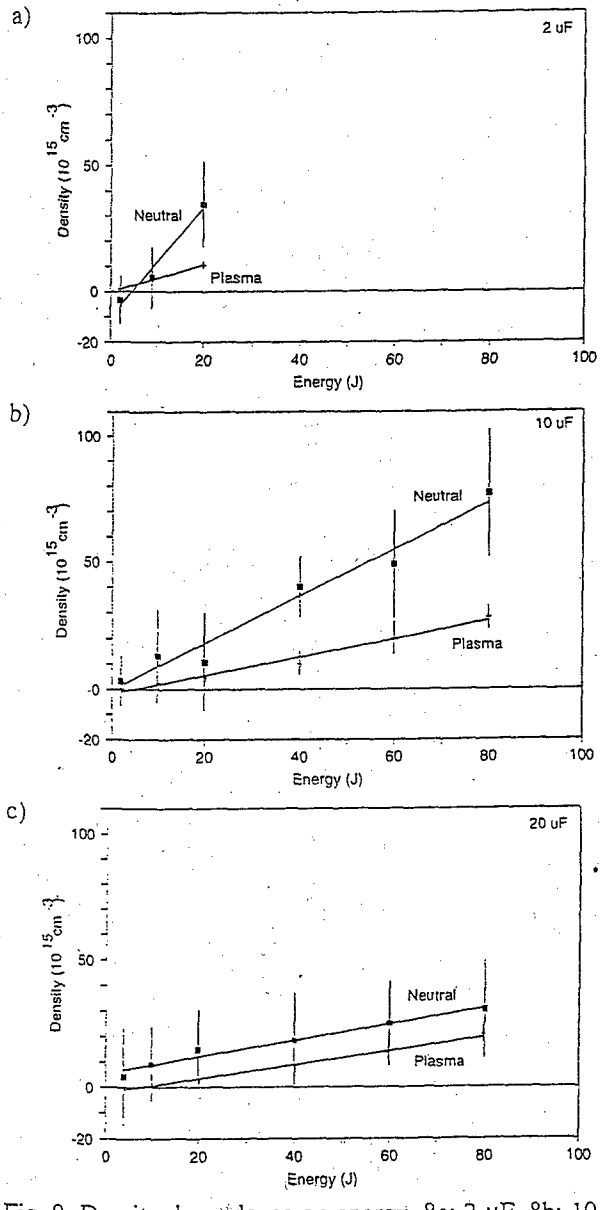

Fig. 9 Density dependence on energy, 8a: 2 μF, 8b: 10 μF, 8c: 20 μF.

The linear scaling of the maximum electron density, coupled with previous measurements showing the same scaling for the total mass usage,[8] implies that increasing the discharge energy will not increase the propellant efficiency. In apparent contradiction is data from LES 8/9 research showing increased thrust efficiency when operating at increased discharge energy.[7] In that work thrust efficiency increased from 7.5% to 13% (not including η_{PPU}), specific impulse increased from 1000 s to 1450 s, and thrust increased from 300 μN to 1500 μN